Supporting Information

Diamond-like $Ag_xCu_{3-x}PS_4$ (x = 1, 2) Synthesized by Metal Oxide-Boron-Chalcogen (MOBQ) Routine: Local High-Entropy Engineering for Balanced Infrared Nonlinear Optical Performance

Ao Guo,[a] Rong-Ling Zhu,[a] Zheng-Ren Chen,[a] Zhi Deng,[a] Zong-Ze Li,[a] Shao-Peng Gui,[a] Mao-Yin Ran[a] and Sheng-Ping Guo*[a,b]

[a]Yunnan Key Laboratory of Electromagnetic Materials and Devices, School of Materials and Energy, Yunnan University, Kunming 650500, P. R. China

[b]Southwest United Graduate School, Kunming 650092, P. R. China

Email: spguo@ynu.edu.cn

Contents

1. Experimental Section

2. Tables

Table S1. Crystal structure refinement parameters for **1** and **2**.

Table S2. Fractional atomic coordinates (× 10^4) and equivalent isotropic displacement parameters (Å^2 × 10^3) for **1** and **2**. U_{eq} is defined as 1/3 of the trace of the orthogonalized U_{ij} tensor.

Table S3. Bond lengths (Å) for **1** and **2**.

Table S4. Bond angles for **1** and **2**.

Table S5. Distortion degrees of polyhedral units in **0**−**2**.

Table S6. Calculated dipole moment results within unit-cells of **0**–**2**.

Table S7. The temperature-dependent ion conductivity for **2**.

Table S8. Comparison of the SHG intensities of the reported M_3PS_4 (M = Ag, Cu and Ag/Cu)[20], and $AgCu_2PS_4$, and Ag_2CuPS_4 reported here.

3. Figures

Figure S1. Rietveld refinement of Powder X-ray diffraction patterns for **1** (a) and **2** (b).

Figure S2. Energy dispersion spectroscopies of **1** (a) and **2** (b).

Figure S3. Crystal photographs of **1** and **2**.

Figure S4. Coordination geometries of Ag/Cu and P atoms in **1** (a) and **2** (b).

Figure S5. The SHG signals of **1**, **2** and $AgGaS_2$ in the particle size of 250−300 μm.

Figure S6. Calculated SHG tensors of **1** (a) and **2** (b).

Figure S7. Calculated band structures (a) and Density of states (b) for **1**. The fermi level is set at 0 eV.

4. References

1. Experimental Section

Syntheses

All starting materials were used as received without further purification. Ag_2S (Aladdin, 99.9 %)，Cu_2O (Aladdin, 99.9 %)，P (Macklin, 98.5 %)，P_2S_5 (Macklin, 99 %)，S (Aladdin, 99.5 %), B (Aladdin, 99.9 %) and KI (Macklin, 99 %). Single crystals of $AgCu_2PS_4$ (**1**) and Ag_2CuPS_4 (**2**) were obtained by the facile metal oxide-boron-chalcogen (MOBQ) solid-state reactions with KI as flux. This method was firstly discovered by Prof. Jin-Shun Huang in 1997, which was then well developed by us from 2008 to now.[1–10]

1: The raw-materials were weighed according to the molar ratios of Ag_2S : Cu_2O : P : S : B = 3 : 6 : 6 : 24 : 4.

2: The raw-materials were weighed according to the molar ratios of Ag_2S : Cu_2O : P_2S_5 : S : B = 6 : 3 : 3 : 9 : 2, and P_2S_5 was weighted in glove box filled with Ar to prevent oxidation and deliquescence.

Each sample has a total mass of 500 mg and additional 400 mg KI.

Each mixture was ground into fine powder in an agate mortar and further pressed into a pellet, followed by being loaded into a quartz tube. The quartz tubes were evacuated to be 1×10^{-4} torr and flame-sealed and then were placed into a muffle furnace, heated from room temperature to 1173 K with several intermediate homogeneous temperatures and kept for 2 days, finally cooled down to 573 K in 5 days, and powered off. The yellow crystals of **1** and **2** were obtained, which were then washed with water and alcohol, followed by being ultrasonic cleaned. These crystals are stable in room temperature for months.

Structure determination

Single-crystal X-ray diffraction (SXRD) data of **1** and **2** were collected by the Bruker D8 QUEST X-ray diffractometer with graphite-monochromated Mo-Kα radiation (λ = 0.71073 Å) at 293 K. The structures were solved by Direct Methods and SHELXL-2014/7 program package within Olex2 v1.5 software were used to solve and refine the crystal structures.[11,12] Crystal data, structure refinement parameters, atomic coordinates and bond lengths are summarized in **Table S1**–**S3**. Their CIF documents were also deposited with the CCDC numbers of 2539219 (**1**) and 2539220 (**2**).

Powder X-ray diffraction (PXRD) analysis

The PXRD patterns were collected by the Bruker D8 Advance diffractometer at 40 kV and 100 mA for Cu-Kα radiation (λ = 1.5406 Å) with a scan speed of 2 ° min^{-1} in room temperature. The simulated PXRD patterns were obtained from single-crystal structure data with the Mercury v3.8 software program provided by the Cambridge Crystallographic Data Center.

UV-vis-NIR diffuse reflectance spectra

The diffuse reflectance spectra were measured on the Cary 5000 UV−vis−NIR spectrometer at room temperature in the wavelength range of 200−2100 nm. The $BaSO_4$ plate was used as the baseline of scanning, on which the finely ground powdery sample was coated.[13] The absorption spectra were calculated from the reflection spectra by the Kubelka-Munk function to obtain the experimental band gaps.[14]

Calculation details

First-principles calculations about the electronic structures and optical properties, and electron localization function (ELF) of **1** and **2** were performed in Materials Studio software base on density functional theory (DFT).[15] The generalized gradient approximation (GGA) by Perdew-Burke-Ernzerhof (PBE) was selected as the exchange-correlation function.[16–17] To ensure the comparability of the results, the computational parameters and convergence criteria for compounds **1** and **2** were maintained identical. The plane-wave cutoff energies for **1** and **2** were both 480.00 eV, and the ultrasoft pseudopotential was selected and the threshold of 5.0 × 10^{-7} eV was set for the self-consistent-field convergence of the total electronic energy. The electrons in $4d^{10}5s^1$, $3d^{10}4s^1$, $3s^23p^3$, $3s^23p^4$ orbitals for Ag, Cu, P, S were regarded as valence electrons. The numerical integration of the Brillouin zones were performed using 4 × 3 × 3 Monkhorst-Pack k-point meshes and the Fermi level at 0 eV was chosen as the reference for **1** and **2**. The real and imaginary parts of the dielectric function were also calculated, which were used to calculated birefringences.[18,19]

Ion conductivity measurement

The electrochemical impedance spectroscopy (EIS) of **2** was measured using an electrochemical workstation (DH7001D) over a frequency range of 1 Hz to 1 MHz. The powder sample was pressed into a pellet with a diameter of 10 mm under a pressure of 380 MPa. The temperature-dependent AC impedance spectroscopy was investigated at variable temperature

from 30 to 80 °C with an increment of 10 °C. The ionic conductivity was calculated via the equation $\sigma = L/(S \cdot R)$, where L is the thickness of the pellet sample and S is its area. The total resistance R is equal to the real impedance when the imaginary impedance approaches zero ($Z'' \approx 0$).

2. Tables

Table S1. Crystal structure refinement parameters for **1** and **2**.

Chemical formula	**$AgCu_2PS_4$ (1)**	**Ag_2CuPS_4 (2)**
Fw (g/mol)	394.20	438.49
T (K)	293	
Crystal system	Orthorhombic	
Space group	$Pmn2_1$	
Z	2	2
***a* (Å)**	7.6319(6)	7.6668(8)
***b* (Å)**	6.2924(4)	6.6063(6)
***c* (Å)**	6.1763(5)	6.3169(5)
***α* (°)**	90	90
***β* (°)**	90	90
***γ* (°)**	90	90
***V* (Å^3)**	296.60(4)	319.95(5)
ρ_{calc} (g cm^{-3})	4.414	4.552
μ (mm^{-1})	11.906	10.775
F(000)	369.0	404.0
2θ range (°)	6.48 to 54.94	6.168 to 49.934
Reflections collected	2292	2302
Indep. reflns/R_{int}	647/0.0435	595/0.0317
GOF on F^2	1.010	1.124
R_1,[a] wR_2[b] (I > 2σ(I))	0.0324, 0.0832	0.0318, 0.0776
R_1,[a] wR_2[b] (all data)	0.0326, 0.0833	0.0337, 0.0788
$\Delta\rho_{max}/\Delta\rho_{min}$, e/Å^3	0.65/−1.33	1.28/−1.44
Flack parameter	0.07(2)	0.01(2)

[a]$R1 = ||F_o| - |F_c||/|F_o|$. [b]$wR2 = [w(F_o^2 - F_c^2)^2] / [w(F_o^2)^2]^{1/2}$.

Table S2. Fractional atomic coordinates (× 10^4) and equivalent isotropic displacement parameters (Å^2 × 10^3) for **1** and **2**. U_{eq} is defined as 1/3 of the trace of the orthogonalized U_{ij} tensor.

Atom	Wyckoff site	*x*	*y*	*z*	U_{eq}[a]/ Å^2
			1		
Ag(1)	2*a*	5000	3527.1(12)	866.2(4)	30.5(3)
Cu(1)	4*b*	7526.1(9)	8138.4(11)	915.5(10)	18.5(3)
P(1)	4*b*	5000	6875(3)	5820(3)	5.9(4)
S(1)	2*a*	7202(2)	8367(2)	4639(2)	12.2(3)
S(2)	2*a*	5000	3725(3)	4907(3)	11.1(4)
S(3)	2*a*	5000	7171(4)	9165(3)	13.6(5)
			2		
Ag(1)	2*a*	5000	6483(3)	4320(4)	55.5(7)
Ag(2)	4*b*	7672.9(17)	1960.3(18)	4020.4(18)	38.1(5)
Cu(1)	4*b*	7672.9(17)	1960.3(18)	4020.4(18)	38.1(5)
P(1)	2*a*	10000	6939(5)	4196(8)	12.0(8)
S(1)	2*a*	5000	2945(7)	5913(7)	19.8(10)
S(2)	4*b*	7816(4)	8418(6)	5253(6)	31.2(8)
S(3)	2*a*	10000	4019(9)	5276(9)	41.2(14)

[a]U_{eq} is defined as one third of the trace of the orthogonalized U_{ij} tensor.

Table S3. Bond lengths (Å) for **1** and **2**.

Bond	Length/Å	Bond	Length/Å
		1	
Ag(1)−S(1)#1	2.5603(17)	Cu(1)−S(2)#5	2.3081(13)
Ag(1)−S(1)#2	2.5603(17)	Cu(1)−S(3)#6	2.2927(13)
Ag(1)−S(2)	2.4988(18)	P(1)−S(1)	2.0588(18)
Ag(1)−S(3)#3	2.522(2)	P(1)−S(2)	2.061(2)
Cu(1)−S(1)#4	2.3451(16)	P(1)−S(3)	2.074(3)
Cu(1)−S(1)	2.3173(18)		
		2	
Ag(1)−S(1)	2.544(5)	Cu(1)−S(2)#2	2.422(4)
Ag(1)−S(2)#1	2.577(4)	Cu(1)−S(2)#3	2.469(4)
Ag(1)−S(2)	2.577(4)	Cu(1)−S(3)	2.380(5)
Ag(1)−S(3)#2	2.576(6)	P(1)−S(2)#5	2.050(4)
Ag(2)−S(1)	2.460(3)	P(1)−S(2)	2.050(4)
Ag(2)−S(3)	2.380(5)	P(1)−S(3)	2.046(6)
Cu(1)−S(1)	2.460(3)	P(1)−S(1)#4	2.076(7)

Symmetry transformations used to generate equivalent atoms: For **1:** $^{\#1}3/2-x$, $1-y$, $-1/2+z$; $^{\#2}-1/2+x$, $1-y$, $-1/2+z$; $^{\#3}+x$, $+y$, $-1+z$; $^{\#4}3/2-x$, $2-y$, $-1/2+z$; $^{\#5}1/2+x$, $1-y$, $-1/2+z$; $^{\#6}1-x$, $+y$, $-1+z$. For **2:** $^{\#1}-x$, $+y$, $+z$; $^{\#2}3/2-x$, $1-y$, $-1/2+z$; $^{\#3}+x$, $-1+y$, $+z$; $^{\#4}2-x$, $+y$, $+z$.

Table S4. Bond angles for **1** and **2**.

Atom	Atom	Atom	Angle/°	Atom	Atom	Atom	Angle/°
				1			
S(1)$^{\#1}$	Ag(1)	S(1)$^{\#2}$	113.02(7)	S(3)$^{\#6}$	Cu(1)	S(2)$^{\#4}$	115.19(6)
S(2)	Ag(1)	S(1)$^{\#2}$	108.60(4)	S(1)$^{\#7}$	P(1)	S(1)	109.43(12)
S(2)	Ag(1)	S(1)$^{\#1}$	108.60(4)	S(2)	P(1)	S(1)	109.98(9)
S(3)$^{\#3}$	Ag(1)	S(1)$^{\#2}$	107.45(4)	S(2)	P(1)	S(1)$^{\#7}$	109.98(9)
S(3)$^{\#3}$	Ag(1)	S(1)$^{\#1}$	107.45(4)	S(3)	P(1)	S(1)	108.18(8)
S(3)$^{\#3}$	Ag(1)	S(2)	111.77(7)	S(3)	P(1)	S(1)$^{\#7}$	108.18(8)
S(2)$^{\#4}$	Cu(1)	S(1)	112.75(7)	S(3)	P(1)	S(2)	111.03(13)
S(2)$^{\#4}$	Cu(1)	S(1)$^{\#5}$	108.25(6)				
S(3)$^{\#6}$	Cu(1)	S(1)	113.25(6)				
S(3)$^{\#6}$	Cu(1)	S(1)$^{\#5}$	99.49(7)				
				2			
S(1)	Ag(1)	S(2)$^{\#1}$	111.41(11)	S(2)	P(1)	S(1)$^{\#2}$	107.9(2)
S(1)	Ag(1)	S(2)	111.41(11)	S(2)$^{\#4}$	P(1)	S(1)$^{\#2}$	107.9(2)
S(1)	Ag(1)	S(3)$^{\#2}$	105.90(19)	S(2)$^{\#4}$	P(1)	S(2)	107.9(2)
S(2)$^{\#1}$	Ag(1)	S(2)	113.79(17)	S(3)	P(1)	S(1)$^{\#2}$	111.6(3)
S(3)$^{\#2}$	Ag(1)	S(2)$^{\#1}$	106.91(11)	S(3)	P(1)	S(2)	109.9(2)
S(3)$^{\#2}$	Ag(1)	S(2)	106.91(11)	S(3)	P(1)	S(2)$^{\#4}$	109.9(2)
S(1)	Cu(1)	S(2)$^{\#3}$	97.73(15)	S(1)	Ag(2)	S(2)$^{\#3}$	97.73(15)
S(2)$^{\#2}$	Cu(1)	S(1)	112.07(13)	S(2)$^{\#2}$	Ag(2)	S(1)	112.07(13)
S(2)$^{\#2}$	Cu(1)	S(2)$^{\#3}$	102.66(11)	S(2)$^{\#2}$	Ag(2)	S(2)$^{\#3}$	102.66(11)
S(3)	Cu(1)	S(1)	108.14(16)	S(3)	Ag(2)	S(1)	108.14(16)
S(3)	Cu(1)	S(2)$^{\#3}$	113.79(15)	S(3)	Ag(2)	S(2)$^{\#2}$	113.79(15)
S(3)	Cu(1)	S(2)$^{\#2}$	120.16(18)	S(3)	Ag(2)	S(2)$^{\#3}$	120.16(18)

Symmetry transformation used to generate equivalent atoms: For **1:**$^{\#1}-1/2+x,\ 1-y,\ -1/2+z$; $^{\#2}3/2-x,\ 1-y,\ -1/2+z$; $^{\#3}+x,\ +y,\ -1+z$; $^{\#4}1/2+x,\ 1-y,\ -1/2+z$; $^{\#5}3/2-x,\ 2-y,\ -1/2+z$; $^{\#6}1-x,\ +y,\ -1+z$; $^{\#7}1-x,\ +y,\ +z$; For **2:** $^{\#1}1-x,\ +y,\ +z$; $^{\#2}3/2-x,\ 1-y,\ -1/2+z$; $^{\#3}+x,\ -1+y,\ +z$; $^{\#4}2-x,\ +y,\ +z$.

Table S5. Distortion degrees of tetrahedral units in **0**–**2**.

Unit	DI (S−M−S)	DI (M−S)	DI (S−S)
	0		
$Cu(1)S_4$	0.010000420	0.01207394	0.00667115
$Cu(2)S_4$	0.03405344	0.00357646	0.02245589
PS_4	0.00691533	0.00247555	0.02442735
	1		
AgS_4	0.01123334	0.009762351	0.011905912
CuS_4	0.0410516	0.00658534	0.023787853
PS_4	0.007920026	0.002605113	0.004967297
	2		
AgS_4	0.0257334	0.004671078	0.016512573
$(Cu/Ag)S_4$	0.0572758	0.01315519	0.034699644
PS_4	0.0095943	0.004804768	0.00519388

Table S6. Calculated dipole moment results within unit-cells of **0**–**2**.

Compound		Dipole moment				
		x	*y*	*z*	Magnitude	
					Debye	× 10^{-4} esu·cm·Å^{-3}
0	**$Cu(1)S_4$**	0	−4.5890	7.1034	8.4568	0.0603
	$Cu(2)S_4$	−0.6992	46.7586	38.0879	60.3120	0.4302
	PS_4	−0.0004	−7.1905	−10.3163	12.5749	0.0897
1	**AgS_4**	−0.0006	−6.6509	15.9535	17.2844	0.1166
	CuS_4	−42.7020	−36.3740	64.0035	85.1057	0.5739
	PS_4	0.0008	−14.2563	−11.0708	18.0500	0.1217
2	**AgS_4**	0	1.3955	−13.9125	13.9823	0.0874
	$(Cu/Ag)S_4$	−5.2170	−37.6707	−74.8507	83.9579	0.5248
	PS_4	0	18.6971	66.539	69.1160	0.4320

Table S7. The temperature-dependent ion conductivity for **2**.

Temperatures / ℃	Ion conductivity / mS/cm
30	9.35×10^{-5}
40	9.00×10^{-5}
50	1.34×10^{-4}
60	4.60×10^{-4}
70	7.08×10^{-4}
80	9.30×10^{-4}

Table S8. Comparison of the SHG intensities of the reported M_3PS_4 (M = Ag, Cu and Ag/Cu)[20], and $AgCu_2PS_4$, and Ag_2CuPS_4 reported here.

Compound	SHG intensity (× AGS)
Cu_3PS_4	0.5 (NPM)
$Ag_{1.5}Cu_{1.5}PS_4$	0.8
Ag_3PS_4	1.3
$AgCu_2PS_4$ (**1**, this work)	0.7
Ag_2CuPS_4 (**2**, this work)	1.1

3. Figures

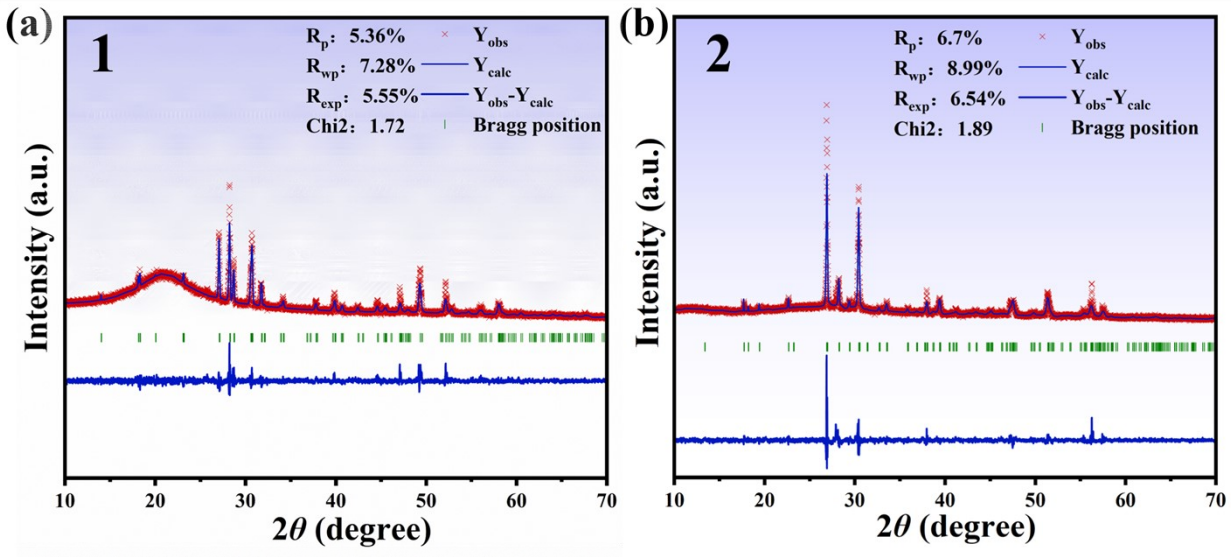

Figure S1. Rietveld refinement of Powder X-ray diffraction patterns for **1** (a) and **2** (b).

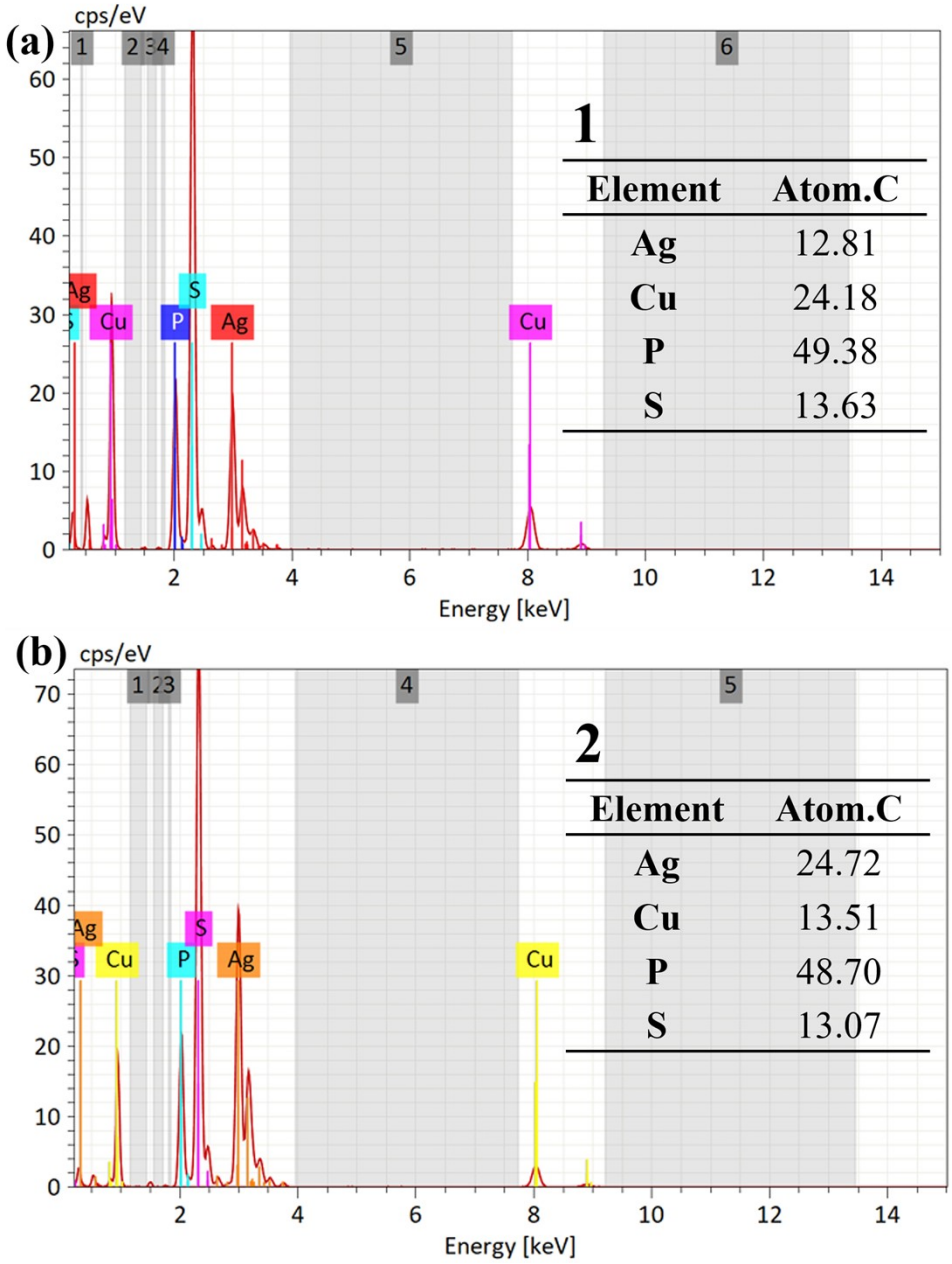

Figure S2. Energy dispersion spectroscopies of **1** (a) and **2** (b). Inset: the molar ratios of component elements.

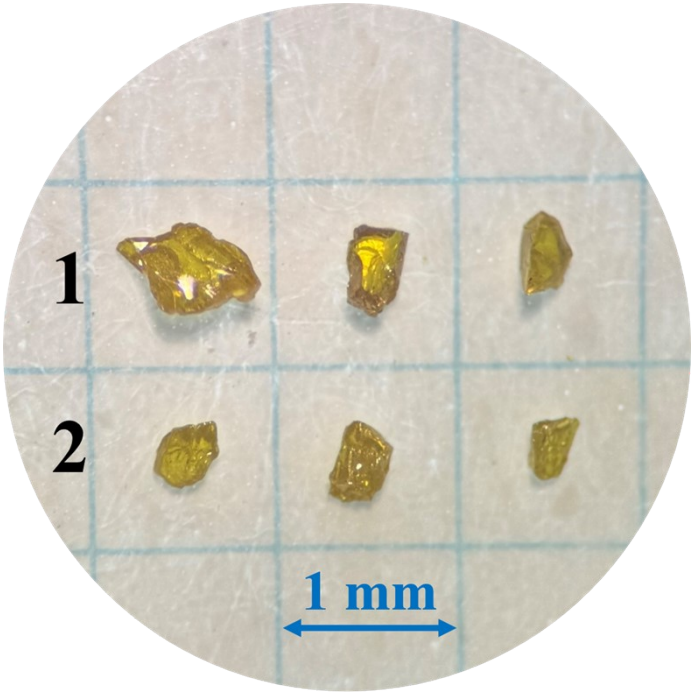

Figure S3. Crystal photographs of **1** and **2**.

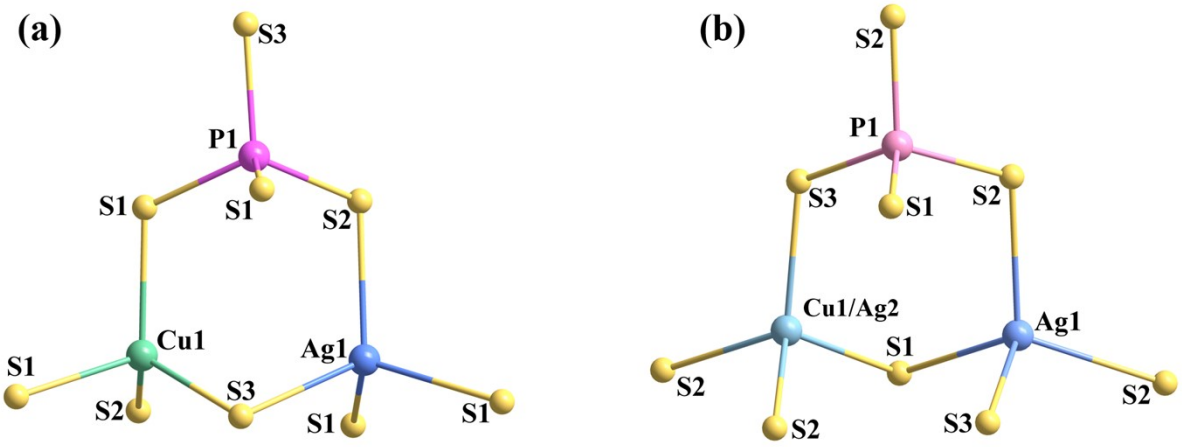

Figure S4. Coordination geometries of Ag/Cu and P atoms in **1** (a) and **2** (b).

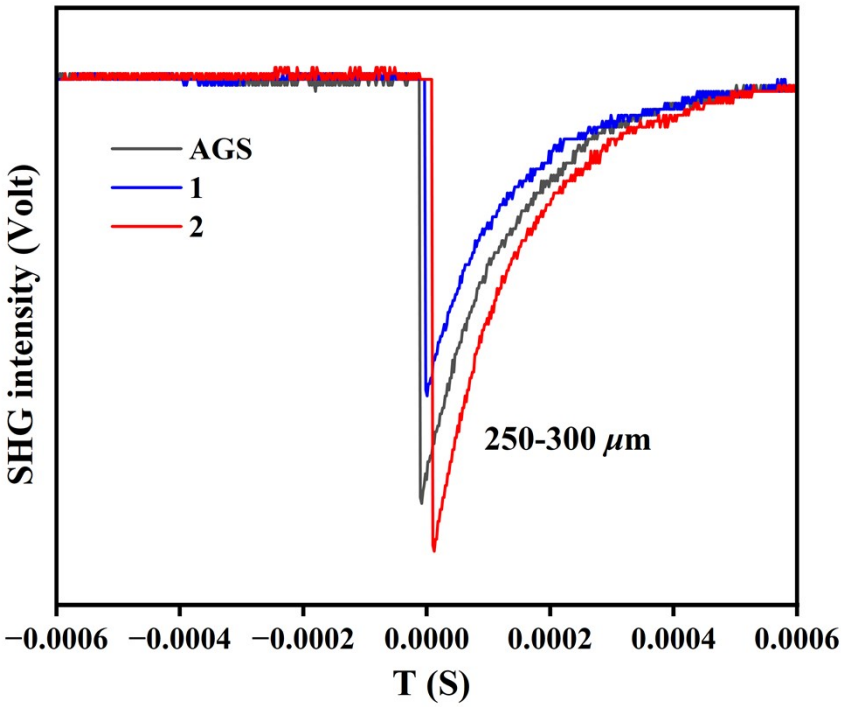

Figure S5. The relative SHG signals of **1**, **2** and $AgGaS_2$ in the particle size of 250−300 μm

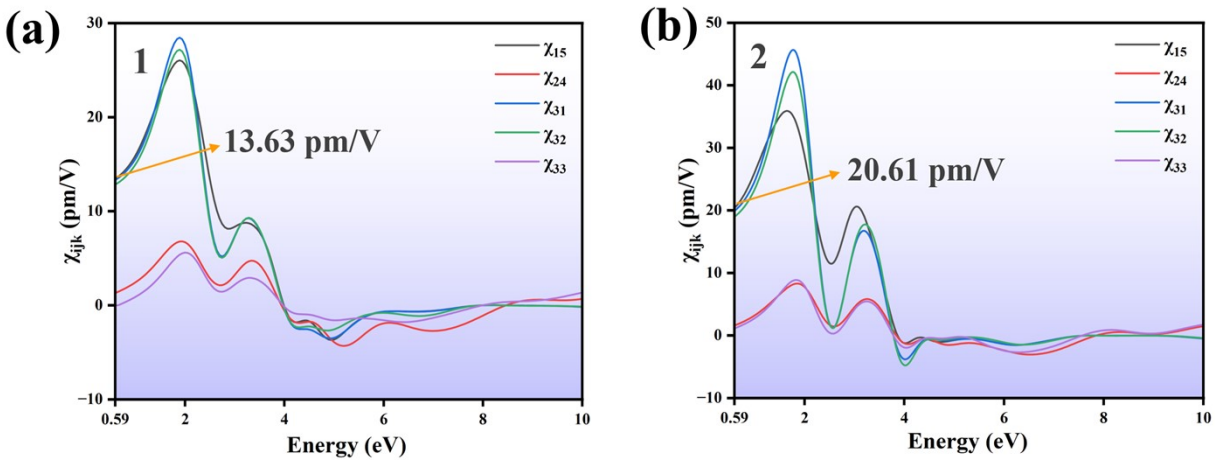

Figure S6. Calculated SHG tensors of **1** (a) and **2** (b).

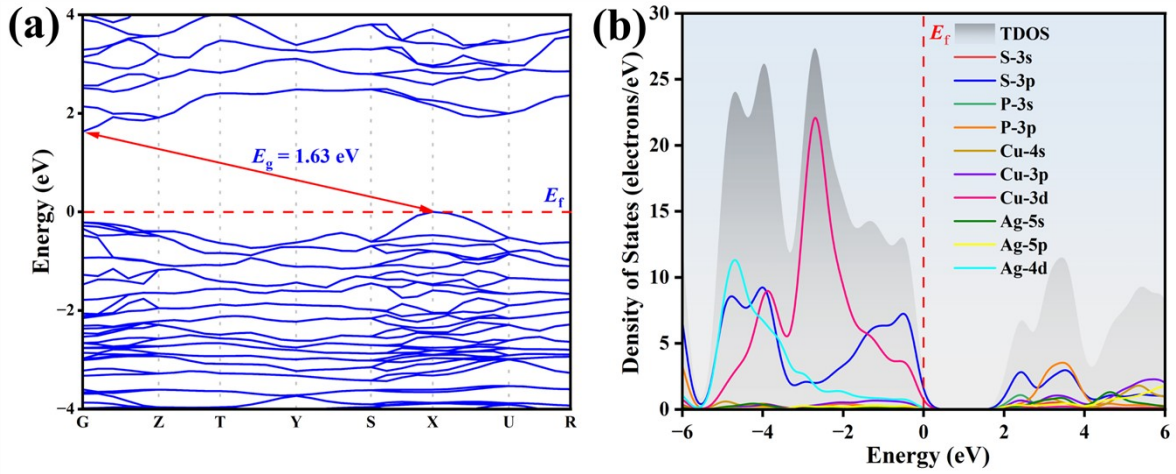

Figure S7. Calculated band structure (a) and density of states (b) for **1**. The fermi level is set at 0 eV.

4. References

(1) S. P. Guo, G. C. Guo, M. S. Wang, J. P. Zou, G. Xu, G. J. Wang, X. F. Long and J. S. Huang, A Series of New Infrared NLO Semiconductors, $ZnY_6Si_2S_{14}$, $Al_xDy_3(Si_yAl_{1-y})S_7$, and $Al_{0.33}Sm_3SiS_7$. *Inorg. Chem.,* 2009, **48**, 7059–7065.

(2) S. P. Guo, G. C. Guo, M. S. Wang, J. P. Zou, H. Y. Zeng, L. Z. Cai and J. S. Huang, A Facile Approach to Hexanary Chalcogenoborate Featuring a 3-D Chiral Honeycomb-like Open-Framework Constructed from Rare-Earth Consolidating Thiogallate-Closo-Dodecaborate. *Chem. Commun.,* 2009, 4366–4368.

(3) S. P. Guo, G. E. Wang, M. J. Zhang, M. F. Wu, G. N. Liu, X. M. Jiang, G. C. Guo and J. S. Huang, Novel Single-Crystal's Voltage-Dependent Effect and Magnetic Order of Ln_2ZrQ_5 (Ln = La, Sm, Gd; Q = S, Se) Semiconductors. *Dalton Trans.,* 2013, **42**, 2679–2682.

(4) S. P. Guo and G. C. Guo, Crystal Structure and Magnetic and Photocatalytic Properties of a New Ternary Rare-Earth Mixed Chalcogenide, $Dy_4S_4Te_3$. *J. Mater. Chem. A.,* 2014, **2**, 20621–20628.

(5) S. P. Guo, Y. Chi and H. G. Xue, $Sm_3S_3BO_3$: The First Sulfide Borate without S–O and B–S Bonds. *Inorg. Chem.,* 2015, **54**, 11052–11054.

(6) X. H. Li, N. T. Suen, Y. Chi, Y. Sun, A. Gong, H. Xue and S. P. Guo, Partial Congener Substitution Induced Centrosymmetric to Noncentrosymmetric Transformation Witnessed by $K_3Ga_3(Ge_{7-x}M_x)Se_{20}$ (M = Si, Sn) and Their Nonlinear Optical Properties. *Inorg. Chem.,* 2019, **58**, 13250–13257.

(7) Z. H. Shi, M. Yang, W. D. Yao, W. Liu and S. P. Guo, $SnPQ_3$ (Q = S, Se, S/Se): A Series of Lone-Pair Cationic Chalcogenophosphates Exhibiting Balanced NLO Activity Originating from SnQ_8 Units. *Inorg. Chem.,* 2021, **60**, 14391–14398.

(8) W. Zhou, W. D. Yao, Q. Zhang, H. Xue and S. P. Guo, Introduction of Li into Ag-Based Noncentrosymmetric Sulfides for High-Performance Infrared Nonlinear Optical Materials. *Inorg. Chem.,* 2021, **60**, 5198–5205.

(9) C. Y. Zhao, C. L. Hu, N. T. Suen, X. H. Li, H. P. Xu, W. Zhou and S. P. Guo, Rare-Earth Substitution Induced Symmetry Breaking for the First Sc-Based Nonlinear Optical Chalcogenide with High-Performance. *Adv. Sci.,* 2025, **12**, 2411960.

(10) Y. Xie, W. D. Yao, Q. Y. Du, W. Zhou, N. T. Suen, W. Liu and S. P. Guo, From $NaSc_3Ga_2Q_8$ (Q = S, Se) to $KGa_2In_3S_8$: Substitution of Sc^{3+} with In^{3+} to Achieve Doubled Birefringence. *Chem. Sci.,* 2025, **16**, 17207–17213.

(11) G. M. Sheldrick, Crystal Structure Refinement with *SHELXL*. *Acta Crystallogr C Struct Chem.,* 2015, **71**, 3−8.

(12) O. V. Dolomanov, L. J. Bourhis, R. J. Gildea, J. A. K. Howard and H. Puschmann, H. OLEX2: A Complete Structure Solution, Refinement and Analysis Program, *J. Appl. Cryst.,* 2009, **42**, 339−341.

(13) W. W. Wendlandt and H. G. Hecht, Reflectance Spectroscopy, Interscience Publishers, *New*

York., 1966.

(14) G. Kortüm, Reflectance Spectroscopy, *Springer.*, 1969.

(15) S. Clark, M. C. Segall, P. Hasnip, M. Probert, K. Refson and M. Payne, First Principles Methods Using CASTEP, Z. *Kristallogr. Cryst. Mater.,* 2005, **220**, 567−570.

(16) M. Gajdoš, K. Hummer, G. Kresse, J. Furthmüller and F. Bechstedt, F. Linear Optical Properties in the Projector-Augmented Wave Methodology, *Phys. Rev. B.,* 2006, **73**, 045112.

(17) J. P. Perdew, K. Burke and M. Ernzerhof, Generalized Gradient Approximation Made Simple. *Phys. Rev. Lett.,* 1996, **77**, 3865−3868.

(18) S. D. Mo and W. Y. Ching, Electronic and Optical Properties of Three Phases of Titanium Dioxide: Rutile, Anatase, and Brookite. *Phys. Rev. B.,* 1995, **51**, 13023–13032.

(19) S. Laksari, A. Chahed, N. Abbouni, O. Benhelal and B. Abbar, First-Principles Calculations of The Structural, Electronic and Optical Properties of $CuGaS_2$ and $AgGaS_2$, *Comp. Mater. Sci.,* 2006, **38,** 223−230.

(20) Y. Yang, B. Zhang, X. Wu and K. Wu, A Series of M_3PS_4 (M = Ag, Cu and Ag/Cu) Thiophosphates with Diamond-like Structures Exhibiting Large Second Harmonic Generation Responses and Moderate Ion Conductivities. *Dalton Trans.,* 2021, **50**, 4129–4132.